The Fifth JSME-KSME Fluids Engineering Conference
Nov. 17-21, 2002, Nagoya, Japan

EFFECTS OF COMBINED SPANWISE AND STREAMWISE ROTATIONS ON TURBULENT CHANNEL FLOW

Haibin Wu and Nobuhide Kasagi
Department of Mechanical Engineering, the University of Tokyo, Hongo 7-3-1, Bunkyo ku, Tokyo 113-8656, Japan
Haibin Wu: wu@thtlab.t.u-tokyo.ac.jp; Nobuhide Kasagi: kasagi@thtlab.t.u-tokyo.ac.jp

Abstract The effects of combined spanwise and streamwise rotation on a turbulent channel flow have been examined through direct numerical simulation. Two cases are considered: constant absolute rotation numbers and a constant spanwise componential rotation number. In the first case, the flow field is generally dominated by the spanwise rotation, but the streamwise rotation effect is appreciable in the spanwise mean velocity and the statistics concerned with the spanwise velocity fluctuation. The changes of friction coefficient and Nusselt number are similar to those in the pure spanwise rotating channel. The ratio of the total heat transfer to the total friction reaches a local maximum at 45°. In the second case, the enhanced turbulence mainly happens along the suction side with increasing the streamwise rotation number, but the spanwise rotating effect is still dominant on the pressure side in the range of the streamwise rotation number considered presently. The ratio of the total heat transfer to the total friction increases more observably for the streamwise rotation number larger than twice the spanwise rotation number.

Keywords turbulent channel flow, system rotation, direct numerical simulation

INTRODUCTION

Rotating turbulent flow exists widely in various industrial, geophysical and astrophysical applications. Understanding the mechanism of such flow in blade passages of turbomachines, for example, should be a key to improve the efficiency of turbomachines. The Coriolis force generated from the system rotation plays a vital role in momentum and heat transfer, so that many researchers have studied the effect of the Coriolis force experimentally and numerically over the several decades.

The carefully designed experiment of spanwise rotating channel flow by Johnston *et al.* [1] revealed that turbulence is enhanced near the pressure side of the channel, but reduced along the suction side. Kim [2] performed large eddy simulation (hereafter LES) of a spanwise rotating channel for a Reynolds number equal to 13,800 (based on the centerline velocity and the channel half-width) and confirmed the stabilized/destabilized effects of the Coriolis force on the two sides of the channel. With direct numerical simulation (hereafter DNS), Kristoffersen and Andersson [3, 4] studied in more details the change of turbulence statistics with the rotation number, based on the friction velocity, which was increased to 7.6 in a spanwise rotating channel. They found that the augmentation and damping of turbulence along the pressure and suction sides, respectively, became more significant with increasing the rotation. Rotation-induced roll cells were also identified.

Applying the lie group analysis of the two-point correlation equations, LES, DNS and second moment turbulent model to a streamwise rotating channel, Oberlack [5] found that both of the streamwise and the induced spanwise mean velocities had the linear scaling laws and all six components of the Reynolds stress tensor were non-zero. Recently, Elsamni and Kasagi [6] carried out systematically DNS of momentum and heat transfer in rotating channels, in which the rotating axis was parallel to one of the three coordinate axes. In their study, the rotation number was increased to 15 for spanwise and streamwise rotating channels and to 0.04 for a wall-normal rotating channel. For the spanwise rotating channel, they reproduced most of the results by Kristoffersen and Andersson [3, 4] and found that the friction coefficient and Nusselt number in the pressure side began to decrease after some critical rotation numbers. The induced spanwise mean velocity in the streamwise rotating channel exhibited increasingly larger peaks, and the friction coefficient and Nusselt number increased monotonously as the rotation number was increased. A large induced spanwise mean velocity was observed in the wall-normal rotating channel and the spanwise bulk mean velocity became much larger for the higher wall-normal rotation number. The friction coefficient and Nusselt number in this case also increased as the rotation number increased.

Most of the former studies mainly focused on the orthogonal rotating cases. In real application, however, the rotating axis is usually not parallel to any of the coordinate axes (see, Fig. 1), so that the Coriolis forces generated from multiple orthogonal components of a rotating vector should interact with each other and make the momentum and heat transfer even more complex. The present work focuses on a comparatively simple case, in which the rotating axis is in the plane parallel to the *x*-*z* plane as shown in Fig. 2, and aims to reveal the combined effects

of spanwise and streamwise rotation on the turbulent channel flow.

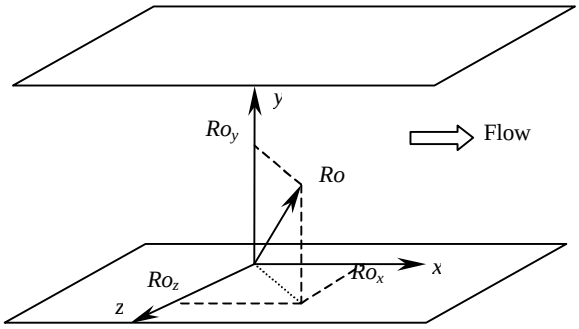

Fig. 1 Channel flow with non-orthogonal system rotation

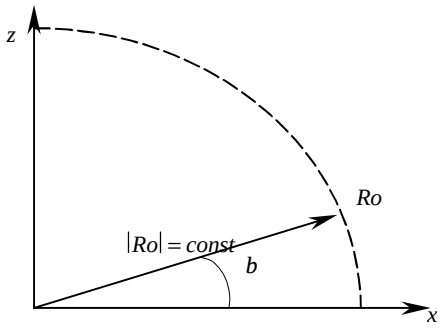

Fig. 2 Rotational vector of combined spanwise and streamwise system rotation in Case I

NUMERICAL SIMULATION METHOD

The momentum and continuity equations with respect to the reference frame rotating with the system at the same speed can be written as follows:

$$\frac{\partial u_i}{\partial t} = -\frac{\partial P}{\partial x_i} + \frac{1}{\mathrm{Re}_t}\frac{\partial^2 u_i}{\partial x_j^2} - u_j\frac{\partial u_i}{\partial x_j} - e_{ijk}Ro_j u_k\,, \qquad (1)$$

$$\frac{\partial u_i}{\partial x_i} = 0\,. \qquad (2)$$

The equations are normalized by the friction velocity u_t and the channel half-width d. The fourth term on the right side of the momentum equation is the Coriolis force due to system rotation. The fully developed turbulent channel flow with a constant streamwise bulk mean velocity and homogeneity in the streamwise x and spanwise z directions are assumed. The temperatures on the two walls are kept constant with Prandtl number Pr equal to 0.71. The Reynolds number Re_b, based on the bulk mean velocity and channel half-width, is set to 4560.

In the present DNS, a $64\times65\times64$ grid system with the computation domain of $5pd\times2d\times2pd$ in the x, y and z directions, respectively, is employed. A pseudospectral method with Fourier series expansion in homogeneous directions and Chebyshev polynomials in the wall-normal direction is used for spatial discretization. The time integration is carried out by employing the Crank-Nicolson scheme for the viscous terms and the Adams-Bashforth scheme for the nonlinear terms. After the flow reaches a fully developed state, in which the total stress across the channel becomes linear, the time integration is extended to $12d/u_t$ for sampling statistics with a time step equal to $0.12d^2/u$.

In the present study, we consider two cases: the absolute rotation number Ro is kept constant in Case I and the spanwise rotation number Ro_z is kept constant in Case II. In the first case, the angle of b between the rotating axis and the x-direction is changed to be five different values, 0, 30, 45, 60 and 90° for each of three different values of Ro. In the second case, the spanwise rotation number Ro_z is set to 2.5 and the streamwise rotation number Ro_x is increased to 15.

RESULTS AND DISCUSSION

Constant absolute rotation number (Case I)

The friction coefficient and Nusselt number normalized by those in a non-rotating channel are plotted in Figs. 3 and 4, respectively. The results in the pure spanwise rotating channel with the rotation number equal to 2.5, 3.5 and 5 are also given in these figures. We can see that, for two different Ro of 7.5 and 11, both of C_f and Nu on the pressure side first increase with b, but after some critical angles they do not increase any more but begin to decrease. The peaks of C_f and Nu on the pressure side appear at 45 and 30° for Ro =7.5 and 11, respectively. For Ro = 5, however, C_f and Nu on the pressure side reach maxima when b is equal to 90°.

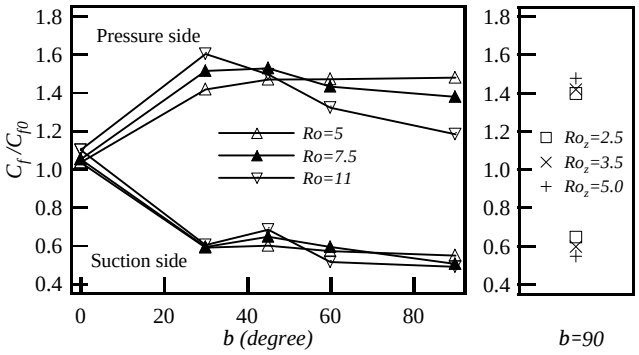

Fig. 3 Friction coefficient in Case I

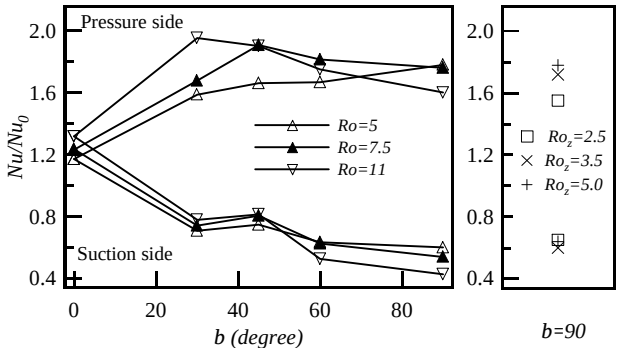

Fig. 4 Nusselt number in Case I

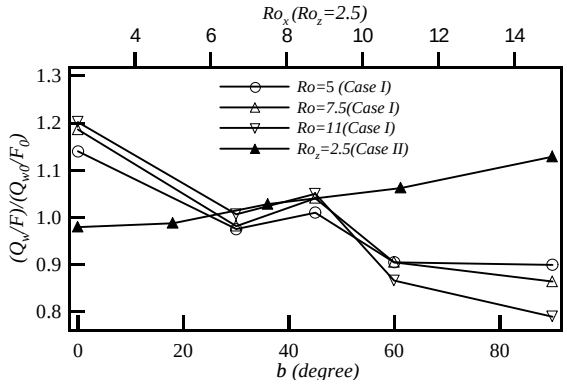

Fig. 5 Ratio of total heat transfer to total friction

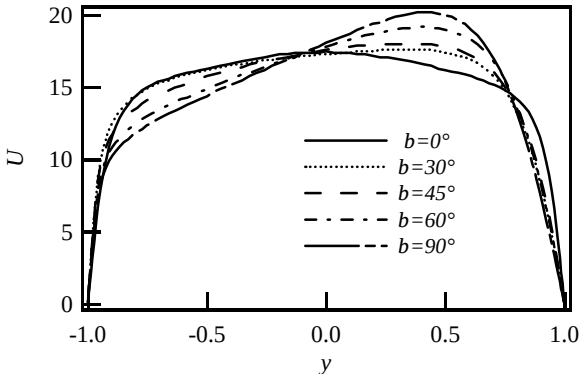

Fig. 6 Streamwise mean velocity in Case I

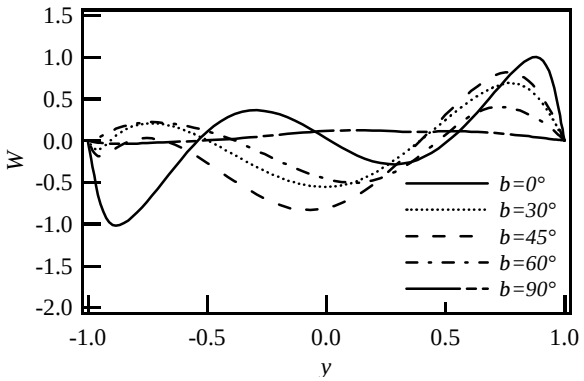

Fig. 7 Spanwise mean velocity in Case I

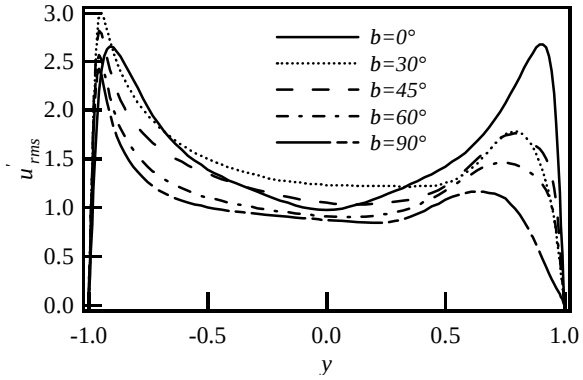

Fig. 8 Rms streamwise velocity fluctuation in Case I

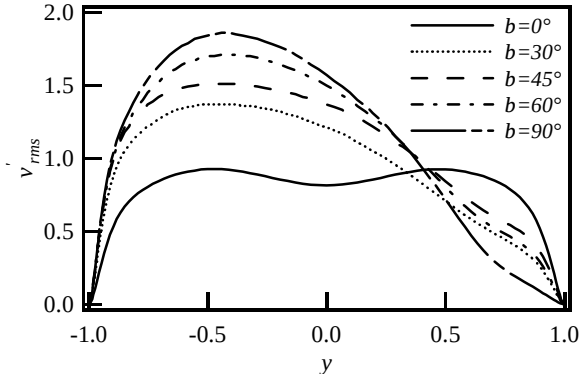

Fig. 9 Rms wall-normal velocity fluctuation in Case I

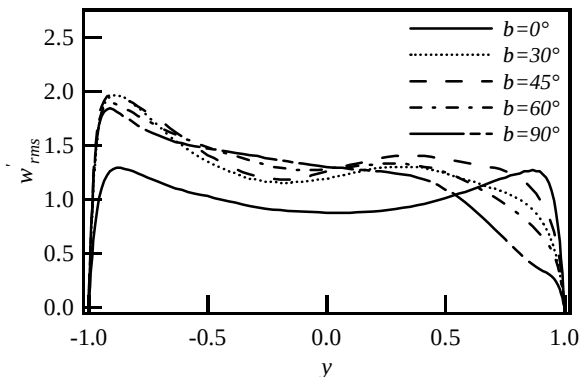

Fig. 10 Rms spanwise velocity fluctuation in Case I

On the suction side, both values first decrease largely as b increases, but then the rate of decrease becomes much slower for b larger than 30°. The changes of C_f and Nu with b are quite similar to those in the pure spanwise rotating channel. At 30°, Ro_z is half of Ro, that is, presently equal to 2.5, 3.75 and 5.5. Compared with those in the pure spanwise rotating channel at Ro_z = 2.5, 3.5 and 5.0, C_f and Nu in Case I are close to them, so that the spanwise component of rotation should be dominant in this case. However, as Ro becomes larger, the difference between Case I and the pure spanwise rotating channel increases, and this means the effect of streamwise rotation is also appreciable. It is very interesting that both the friction coefficient and Nusselt number have local peaks around 45° on the suction side. The ratio of the total heat transfer Q_w to the total friction F reaches a local maximum value at 45° as shown in Fig. 5.

The streamwise and spanwise mean velocities are shown in Figs. 6 and 7. Here, only the results for Ro = 7.5 are represented; those for the other two rotation numbers have a similar tendency. The change of the streamwise mean velocity is quite similar to that in the pure spanwise rotating channel. The linear regime has larger slope as b increases, so that the profile of the streamwise mean velocity is mainly determined by the spanwise rotation. The change of the spanwise mean velocity is quite complicated. At b =0°, that is, the pure streamwise rotating channel, the spanwise mean velocity is skew-symmetric, two extreme values appear near the two walls and two cambers with different signs occupy the central region of the channel. Excluding b =90°, at which the spanwise mean velocity is almost zero, the absolute value of the extreme near the pressure side becomes very small as well as the peak near the suction side also decreases for b = 30, 45 and 60°. The camber near the pressure side moves toward

the pressure wall and becomes much smaller, but the camber near the suction side expands largely and its absolute value increases. Among these three angles, the camber near the suction side becomes largest and its absolute value reaches maximum at 45°.

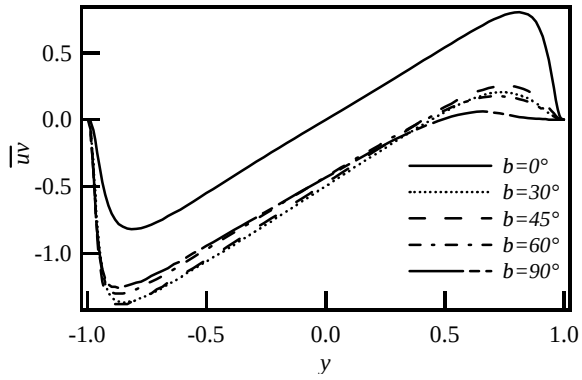

Fig. 11 Reynolds shear stress component $\overline{uv}$ in Case I

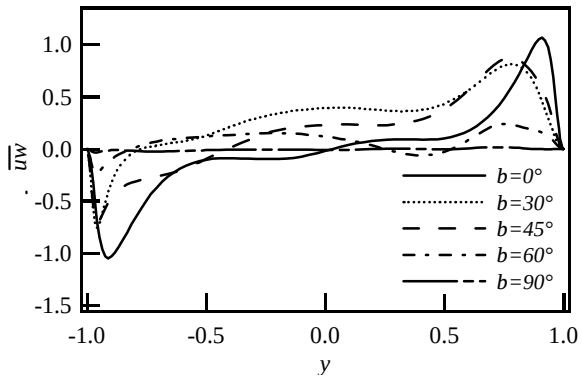

Fig. 12 Reynolds shear stress component $\overline{uw}$ in Case I

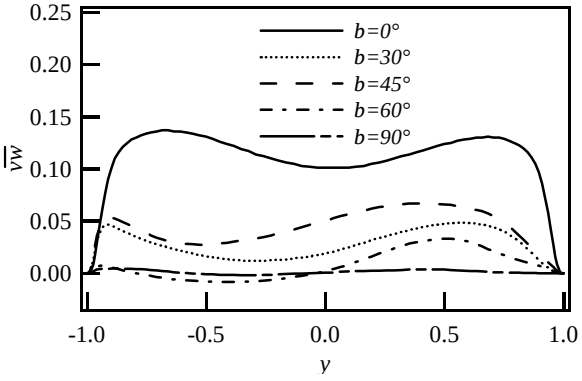

Fig. 13 Reynolds shear stress component $\overline{vw}$ in Case I

The root mean square (hereafter rms) values of the velocity fluctuations are shown in Figs. 8, 9 and 10. The rms streamwise and wall-normal velocity fluctuations have similar tendencies to those in the pure spanwise rotating channel. The suppression of u'_{rms} near the pressure side for b larger than 30° and the continuous decrease on the suction side strongly suggest the dominant effect of the spanwise rotation. Furthermore, the consecutive augmentation near the pressure side and reduction along the suction side of v'_{rms} with b also reveal the dominance of spanwise rotating effect. However, the change of w'_{rms} is not similar to that in the pure spanwise rotating channel. We can see that this quantity near the pressure side reaches a maximum value at 30° and then decreases. Near the suction side, however, this term first decreases, recovers at 45°, and then reduces again.

The three off-diagonal components of the Reynolds stress terms are shown in Figs. 11, 12 and 13. In the pure streamwise rotating channel, $\overline{uv}$ and $\overline{uw}$ are skew-symmetric and $\overline{vw}$ is symmetric with respect to the center of the channel. In the pure spanwise rotating channel, $\overline{uv}$ is non-zero, but the other two terms are zero. For the present case, the enhancement of the Reynolds stress $\overline{uv}$ on the pressure side and the suppression on the suction side denote the strong effect of spanwise rotation. For the other two terms, $\overline{uw}$ and $\overline{vw}$, their values approach to zero as b increases. In the attenuation process, however, there is a rebound at 45°, and these two terms are no longer skew-symmetric or symmetric with respect to the center of the channel.

From these statistics, it is shown that the spanwise rotating effect dominates the flow field, so that many tendencies are quite similar to those in the pure spanwise rotating channel. However, the effect of streamwise rotation can not be neglected, since the spanwise mean velocity and the statistics concerned with spanwise velocity fluctuation are influenced appreciably by the streamwise rotation.

Constant spanwise rotation number Ro_z (Case II)

In Case II, with a constant spanwise rotation number Ro_z = 2.5, the streamwise rotation number Ro_x is increased to 15, as shown in Fig. 14.

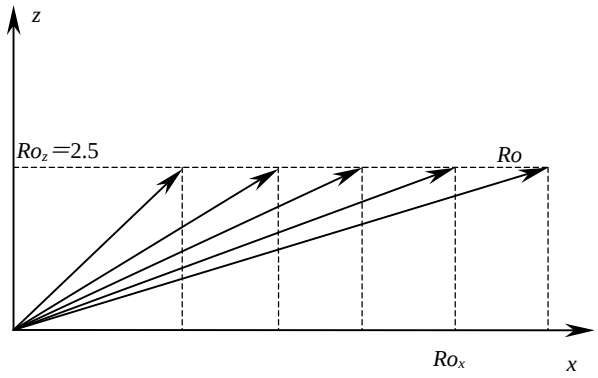

Fig. 14 Rotational vector of combined spanwise and streamwise system rotation in Case II (not the real scale)

The friction coefficient and Nusselt number in Case II are shown in Figs. 15 and 16. The Nusselt number on both sides and the friction coefficient on the suction side clearly increase beyond Ro_x = 5, while the friction coefficient on the pressure side increases only slightly. It is known that C_f and Nu increase when the streamwise rotation number becomes larger in the pure streamwise rotating channel. Therefore, the present results reveal that C_f near the suction side and Nu on both sides are evidently influenced by the streamwise rotation when Ro_x is larger than twice Ro_z. The friction coefficient near the pressure

side is still dominated by spanwise rotating effect and the influence of streamwise rotation is secondary. The ratio of the total heat transfer Q_w to the total friction F increases more observably for Ro_x larger than 5 as shown in Fig. 5.

The streamwise and spanwise mean velocities are plotted in Figs. 17 and 18. The gradient of streamwise mean velocity along the suction side increases as Ro_x is increased. The drastic change of the spanwise mean velocity indicates the obvious increase of the streamwise rotation effect. This term, however, on the suction side is much more remarkable than that near the pressure side.

The rms velocity fluctuations are shown in the Figs. 19, 20 and 21. The increase of turbulent intensities along the suction side reveals the increasing effect of streamwise rotation, but near the pressure side these values are almost constant, which reveals that the spanwise rotation effect is still dominant on this side.

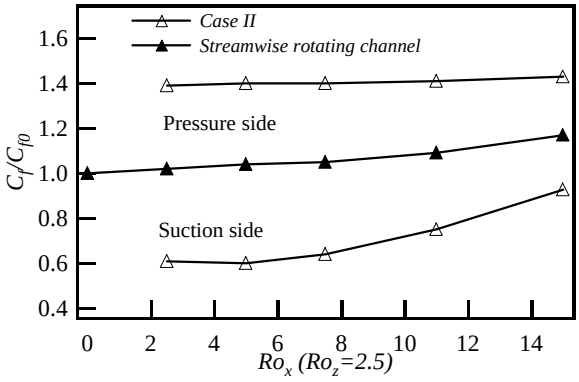

Fig. 15 Friction coefficient in Case II

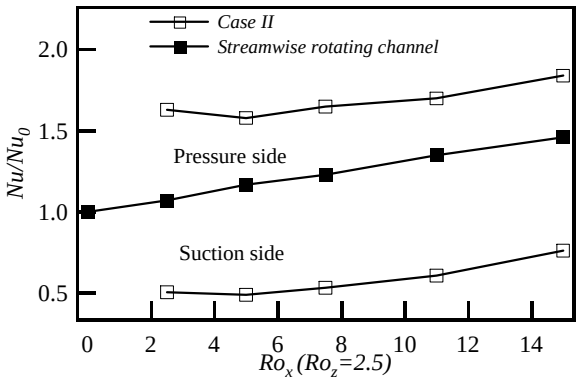

Fig. 16 Nusselt number in Case II

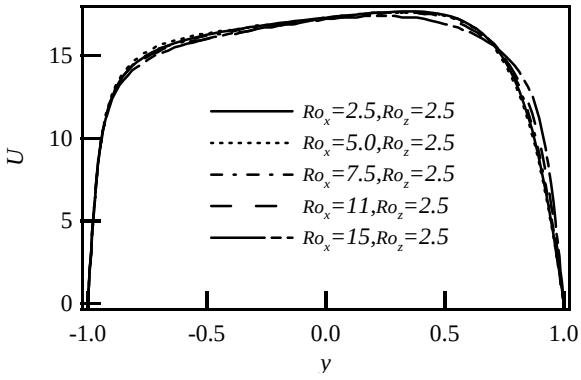

Fig. 17 Streamwise mean velocity in Case II

The increasing streamwise rotation effect near the suction side can also be seen in the Reynolds stress term $\overline{uv}$ as shown in Fig. 22. It is almost constant along the pressure side, but increases drastically near the suction side; this results in the

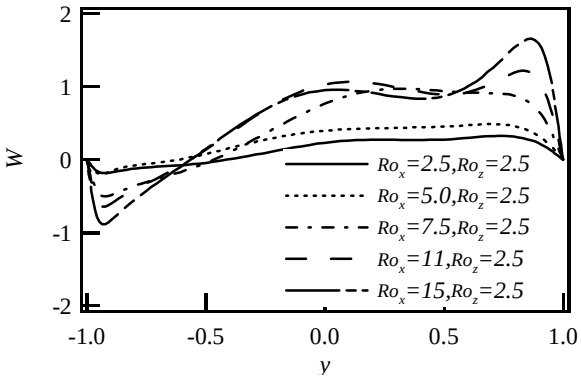

Fig. 18 Spanwise mean velocity in Case II

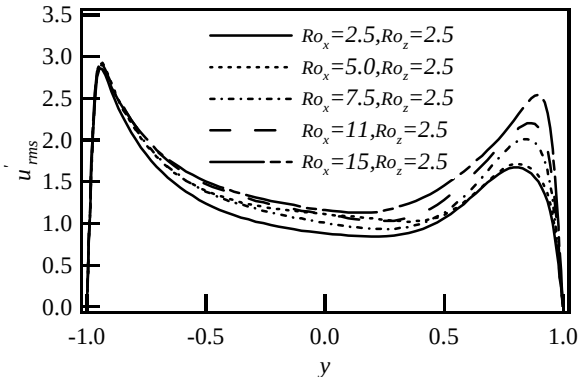

Fig. 19 Rms streamwise velocity fluctuation in Case II

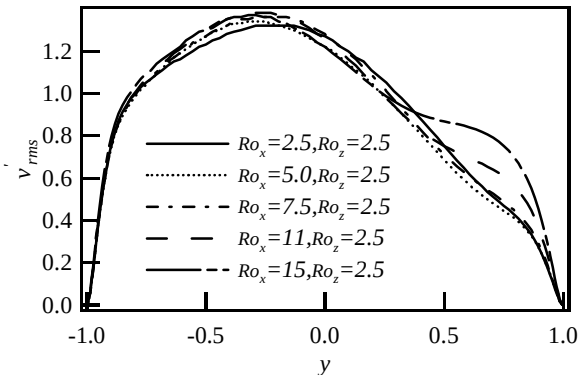

Fig. 20 Rms wall-normal velocity fluctuation in Case II

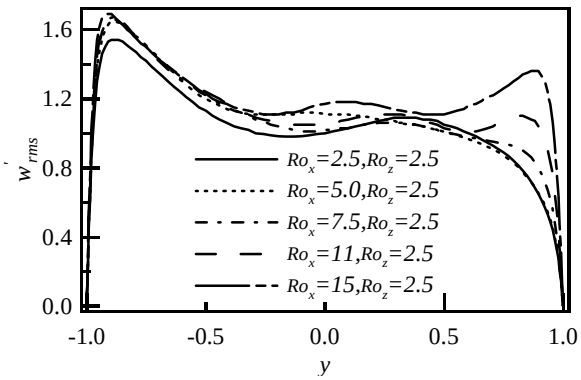

Fig. 21 Rms spanwise velocity fluctuation in Case II

remarkable enhancement of turbulence on the suction side.

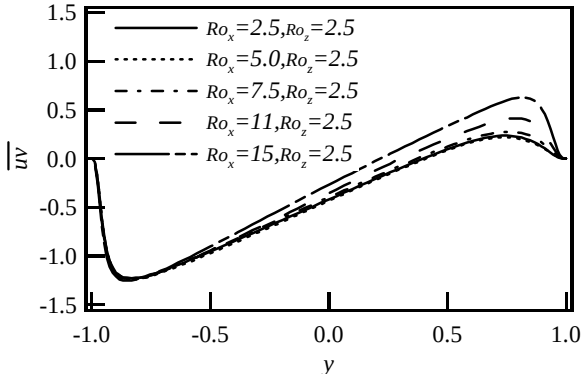

Fig. 22 Reynolds shear stress component $\overline{uv}$ in Case II

CONCLUSIONS

In the present study, a series of DNS have been performed to investigate the combined effect of spanwise and streamwise rotation on a turbulent channel flow. If the absolute rotation number *Ro* is kept constant and only the angle b between rotating axis and *x*-direction is changed, the spanwise rotating effect dominates the flow field for b equal to 30, 45 and 60°. The effect of streamwise rotation is generally minor, but appreciable in the spanwise mean velocity and the statistics concerned with the spanwise velocity fluctuation. Both of the friction coefficient and Nusselt number have weak local peaks around 45° near the suction side. As for the ratio of the total heat transfer to the total friction in the channel, the local maximum values exist at 45°.

When the spanwise rotation number Ro_z is kept constant and only the streamwise rotation number Ro_x is increased, the effect of streamwise rotation begins to enhance the turbulence mainly along the suction side when Ro_x is larger than twice Ro_z. However, on the pressure side, the flow field is still dominated by the spanwise rotation effect in the range of streamwise rotation number considered presently. The ratio of the total heat transfer to the total friction increases more evidently for Ro_x larger than twice Ro_z.

In the present work, the turbulent statistics have been discussed. The flow structure is being studied in details with the aid of visualization and will be represented elsewhere.

ACKNOWLEDGEMENTS

This work was supported through the research project on “Micro Gas Turbine/Fuel Cell Hybrid-type Distributed Energy System” by the Department of Core Research for Evolutional Science and Technology (CREST) of the Japan Science and Technology Corporation (JST).

NOMENCLATURE

C_f	friction coefficient, $C_f = 2t_w / rU_m^2$
F	Total friction across the channel $F = t_{wp} + t_{ws}$
Nu	Nusselt number, $Nu = -2dQ_w/(T_m - T_w)l$
Pr	Prandtl number
Q_w	Total heat transfer across the channel $Q_w = -l(dT/dy)_w$
Re_b	Reynolds number, $\mathrm{Re}_b = 2U_m d/u$
Re_t	Reynolds number, $\mathrm{Re}_t = u_t d/u$
Ro	absolute rotation number, $Ro = 2d\Omega/u_t$
Ro_i	rotation number in *i*-th direction $Ro_i = 2d\Omega_i/u_t$
U, W	streamwise and spanwise mean velocities
u', v', w'	velocity fluctuation in *x*,*y* and *z* directions
u_i	Velocity component in *i*-th direction
u_t	friction velocity

Greek symbols

t	shear stress
Ω	angular velocity of system rotation
d	channel half-width
l	thermal conductivity
b	the angle between the absolute between the rotating axis and *x* direction
u	kinematic viscosity

Subscript and superscript

m	bulk averaged
w	value on the wall
p	value on the pressure side
s	value on the suction side
i	*i*-th direction

REFERENCES

[1] Johnston, J. P., Halleen, R. M., and Lezius, D. K., Effects of Spanwise Rotation on the Structure of Two-dimensional Fully Developed Turbulent Channel Flow, J. Fluid Mech., Vol. 56, Part 3, 533-557 (1972).

[2] Kim, J., The Effect of Rotation on Turbulence Structure, Proc. 4th Symp. Turbulent Shear Flows, Karlsruhe, 6.14-6.19 (1983).

[3] Kristoffersen, R., and Andersson, H. I., Direct Simulation of Low Reynolds-number Turbulent Flow in A Rotating Channel, J. Fluid Mech., Vol. 256, 163-197 (1993).

[4] Andersson, H. I., and Kristoffersen, R., Turbulence Statistics of Rotating Channel Flow, Proc. 9th Symp. Turbulent Shear Flows, Kyoto, 53-70 (1993).

[5] Oberlack, M., Cabot, W., and Rogers, M. M., Turbulent Channel Flow with Streamwise Rotation; Lie Group Analysis, DNS and Modeling, 1st Int. Symp. Turbulence & Shear Flow Phenomena, Santa Barbara, 85-90 (1999).

[6] El-Samni, O., and Kasagi, N., The Effects of System Rotation with Three Orthogonal Rotating Axes on Turbulent Channel Flow, 7th Int. Cong. Fluid Dyn. & Prop., Cairo, CD-ROM, ASME (2001).